

Biomaterials Science

Accepted Manuscript

This article can be cited before page numbers have been issued, to do this please use: J. Guo, T. Li, Z. Hu, C. Wang, J. Yang, C. Zeng and R. Fan, *Biomater. Sci.*, 2020, DOI: 10.1039/C9BM01575B.



This is an Accepted Manuscript, which has been through the Royal Society of Chemistry peer review process and has been accepted for publication.

Accepted Manuscripts are published online shortly after acceptance, before technical editing, formatting and proof reading. Using this free service, authors can make their results available to the community, in citable form, before we publish the edited article. We will replace this Accepted Manuscript with the edited and formatted Advance Article as soon as it is available.

You can find more information about Accepted Manuscripts in the [Information for Authors](#).

Please note that technical editing may introduce minor changes to the text and/or graphics, which may alter content. The journal's standard [Terms & Conditions](#) and the [Ethical guidelines](#) still apply. In no event shall the Royal Society of Chemistry be held responsible for any errors or omissions in this Accepted Manuscript or any consequences arising from the use of any information it contains.

PD-L1-targeted microbubbles loaded with docetaxel produce a synergistic effect for the treatment of lung cancer under ultrasound irradiation

Tiankuan Li^{1†}, Zhongqian Hu^{2†}, Chao Wang¹, Jian Yang³, Chuhui Zeng¹, Rui Fan¹, Jinhe Guo^{1*}

¹ Center of Interventional Radiology and Vascular Surgery, Department of Radiology, Zhongda Hospital, Medical School, Southeast University, Nanjing, China

² Department of Ultrasound, Zhongda Hospital, Medical School, Southeast University, Nanjing, China

³ Jiangsu Key Laboratory of Molecular and Functional Imaging, Department of Radiology, Zhongda Hospital, Medical School, Southeast University, Nanjing, China

† These authors contributed equally to this work.

*Corresponding Author: Dr. Jinhe Guo, Email: jinheguo@sina.com, Center of Interventional Radiology and Vascular Surgery, Department of Radiology, Zhongda Hospital, Medical School, Southeast University, 87 Dingjiaqiao Road, Nanjing 210009, China



Abstract:

Immunotherapy is gradually becoming as important as traditional therapy in the treatment of cancer, but adverse drug reactions limit patient benefits from PD1/PD-L1 checkpoint inhibitor drugs in the treatment of non-small cell lung cancer (NSCLC). As a chemotherapeutic drug for NSCLC, docetaxel (DTX) can synergize with PD1/PD-L1 checkpoint inhibitors but increase haematotoxicity and neurotoxicity. Herein, anti-PD-L1 monoclonal antibody (mAb)-conjugated and docetaxel-loaded multifunctional lipid-shelled microbubbles (PDMs), which were designed with biological safe phospholipid to produce synergistic antitumour effects, reduced the incidence of side effects and promoted therapeutic effects under ultrasound (US) irradiation. The PDMs were prepared by the acoustic-vibration method and then conjugated with an anti-PD-L1 mAb. The material features of the microbubbles, cytotoxic effects, cellular apoptosis and cell cycle inhibition were studied. A subcutaneous tumour model was established to test the drug concentration-dependent and antitumour effects of the PDMs combined with US irradiation, and an orthotopic lung tumour model simultaneously verified the antitumour effect of this synergistic treatment. The PDMs achieved higher cellular uptake than free DTX, especially when combined with US irradiation. The PDMs combined with US irradiation also induced an increased rate of cellular apoptosis and an elevated G2-M arrest rate in cancer cells, which was positively correlated with PD-L1 expression. An in vivo study showed that synergistic treatment had relatively strong effects on tumour growth inhibition, increased survival time and decreased adverse effect rates. Our study possibly provides a well-controlled design for immunotherapy



and chemotherapy and has promising potential as a clinical application for NSCLC treatment.

Keywords: immunochemotherapy, microbubble, ultrasound irradiation, non-small cell lung cancer, drug delivery

Introduction

Lung cancer is the type of cancer with the highest morbidity and mortality worldwide¹, and NSCLC is the main type of lung cancer². For the past few years, the most exciting antitumour drug class has been PD1/PD-L1 checkpoint inhibitors, which can counteract the abilities of tumour cells to suppress the immune system and promote self-tolerance³⁻⁵. Due to its broad application, immunotherapy has become as valid as chemotherapy for advanced NSCLC^{6, 7}. Clinical evidence has shown that the combination of a PD1/PD-L1 checkpoint inhibitor with a chemotherapeutic drug can achieve better therapeutic effects than monotherapy^{8,9}. However, in addition to the cardiotoxicity of PD1/PD-L1 checkpoint inhibitors^{10,11}, this combination of free drugs also aggravates haematotoxicity, hepatotoxicity, and neurotoxicity^{12,13}. Therefore, an appropriate drug delivery system is needed to reduce the adverse events of these two drugs.

Drug delivery systems based on microbubbles are good contrast agents and drug carriers and have the advantages of satisfactory chemical stability, biodegradability, low toxicity, and easy chemical modification¹⁴. The common components of the microbubble shell are albumin, phospholipids, and macromolecular polymers. Clinical studies have shown that lung surfactant microbubbles increase lipophilic drug payloads



for ultrasound (US)-targeted delivery¹⁵. Microbubbles' smaller size allows extravasation from blood vessels into surrounding tissues, improving stability and giving longer residence times in the systemic circulation¹⁶. Therefore, lipid-shelled microbubbles might be an appropriate drug delivery system for the combination of a PD1/PD-L1 checkpoint inhibitor and docetaxel (DTX).

As one of the most common noninvasive physical radiation sources, US plays an important role in clinical diagnosis and therapy. Lung US as an emerging theranostic modality exhibits non-ionizing properties, high local resolution, real-time imaging, and low cost¹⁷. Clinical trials have verified the efficacy and safety of pulmonary US irradiation treatment combined with corresponding drugs^{18, 19}. The cavitation and sonoporation effects are generally believed to contribute to the therapeutic effect of US irradiation, which can ensure specialized targeted delivery of proteins, genes, exosomes or traditional chemotherapeutic drugs²⁰⁻²². Hence, we hypothesized that immunochemotherapeutic phospholipid microbubbles combined with US irradiation might enhance the efficacy and reduce the adverse effects of the combination of a PD1/PD-L1 inhibitor and DTX.

To verify our hypothesis, we designed a multifunctional microbubble system in which the membrane was DTX loaded and then anti-PD-L1 monoclonal antibody (mAb)-modified (PDMs). The anti-PD-L1 mAb could block the immunosuppressive PD1/PD-L1 pathway, while the PDMs directly kill tumour cells via DTX. Moreover, US irradiation was used to rupture the PDMs to further increase drug concentrations in the tumour. The cavitation and sonoporation effects improve the ability of drugs to enter

View Article Online
DOI: 10.1039/C9BM01575B



the interstitial space and tumour cells. Our study showed that the PDMs had excellent antitumour activity both *in vitro* and *in vivo*. Fluorescence microscopy and flow cytometry showed that PDM treatment led to increased DTX uptake, which enhanced cellular apoptosis and cell cycle inhibition. The distribution of DTX and PD-L1 in tumour tissues was also observed by *in vivo* fluorescence imaging. Our results revealed that the PDMs could not only increase the effect of chemotherapy but also enhance the antitumour effect by promoting the proliferation of CD4⁺ T and CD8⁺ T cells and decreasing the levels of the cytokines VEGF, TNF- α , and TGF- β . All these outcomes indicated that the PDMs had good antitumour efficacy.

Results and Discussion

Characterization of immunochemotherapeutic microbubbles

The synthesis process for the PD-L1-mediated immunochemotherapeutic microbubbles is summarized in Fig. 1A. A schematic diagram showing the US irradiation-enhanced drug cytotoxicity and immune-activating mechanism of the microbubbles is presented in Fig. 1B. The microbubbles' round shape was manifested by a scanning electron micrograph (Fig. 2A). The sizes of the microbubbles are shown in Table S1; Blank microbubble (BM) size was initially 607.6 ± 22.7 nm with a polydispersity index (PDI) of 0.234 ± 0.018 and zeta potential of -3.91 ± 0.861 mV. The size of microbubbles later increased to 629.1 ± 19.8 nm with a PDI of 0.259 ± 0.026 and zeta potential of -8.98 ± 0.693 mV after loading DTX. The parameters further increased to 666.4 ± 35.9 nm with a PDI of 0.298 ± 0.036 and zeta potential of $-9.69 \pm$



0.964 mV after coupling to an anti-PD-L1 mAb. These increases were concluded to be the result of successful synthesis of the antibody. The dispersions of the microbubbles are shown in Fig. 2B. The change in size could be a sign of successful binding of the antibody to the surface of the microbubbles. The encapsulation and loading efficiency of DTX in the DTX-loaded microbubble (DM) were $59.21 \pm 1.97\%$ and $4.75 \pm 0.65\%$, respectively, and in the PDMs were $57.34 \pm 2.61\%$ and $4.45 \pm 0.91\%$, respectively (Table S2).

The profiles of the release of DTX from the microbubbles with/without US irradiation were examined to assess the effects of sonication on DTX release. As shown in Fig. 2C, US irradiation significantly promoted drug release. CY5-labelled anti-PD-L1 mAb conjugation with FITC-labelled DTX microbubbles were observed by the laser scanning confocal microscopy (LSCM) (Fig. 2D). The microbubbles consistently maintained a round shape and were bound with a fluorescein-labelled antibody.

The BMs, DMs, and PDMs had similar contrast imaging capabilities *in vitro* and *in vivo* (Fig. 2E); the peak intensity and time to peak were not significantly different among the microbubbles (Fig. 2F and Fig. 2G). In addition to the expression on a number of cancer cell lineages, PD-L1 was also expressed on non-parenchymal cells and non-haematopoietic lineages⁵. The distribution of PD-L1 in other organs might prevent the enhancing effect of the microbubbles from being obvious over a short period of time.

We also investigated whether BMs, DMs, and PDMs can induce haemolysis (Fig. S1A and B), the result showed none of the formulations was haemolytic. The toxicity



study showed that no weight loss was observed, and serum biochemical parameters were within the corresponding reference ranges (Fig. S2A-E). HE staining showed that the free combo group resulted in thickened alveolar walls and lymphocyte infiltration in normal lung tissue. Our findings illustrate the immunochemotherapeutic microbubbles are biologically safe and lung protective.

Microbubble cytotoxicity in vitro

The PD-L1 expressions of one type of mouse cell (LLC) and three types of human cells (NCI-H460, NCI-H1299, and A549) were tested by flow cytometry. As shown in Fig. 3A and B, the expression of LLC cells was similar to that of NCI-H460 cells, while NCI-H1299 cells had the highest expression and A549 cells had the lowest. Free DTX and DMs had similar cytotoxicity in the four tumour cell lines. PDMs had stronger efficacy because of the conjugated anti-PD-L1 mAb, and this efficacy was strengthened by US irradiation (Fig. 3C-F). The results demonstrated that anti-PD-L1 mAb targeting and US irradiation could both enhance the cytotoxicity of DTX to the target tumour tissues.

***In vitro* enhancement of cellular drug uptake mediated by PD-L1**

To further assess the relationship between the targeting efficiency of PDMs and affinity of DTX for LLC cells *in vitro*, the cellular uptake of DTX in different formulations was determined by fluorescence imaging and flow cytometry. C6 to indicate drug uptake was contained in microbubbles at a concentration equimolar to DTX. As shown in Fig. 3A and D, CLSM images indicated elevated intracellular drug uptake of C6-PDMs, especially with US irradiation. The flow cytometry results were also consistent with the



fluorescence imaging results (Fig. S4). Therefore, PD-L1–mediated internalization was more efficient than passive diffusion and nonspecific target. US irradiation could promote drug uptake, which might account for the increased cellular toxicity of PDMs when combined with US irradiation.

Apoptosis induction and cell cycle inhibition in LLC cells in vitro

The cell apoptosis study assessing different formulations utilized the Annexin V-FITC/PI method to further explore tumour killing. LLC cells were treated with US irradiation, free DTX, DMs, PDMs, or PDMs + US. After 24 h of incubation, the total apoptosis rate was analysed by flow cytometry. As shown in Fig. 3B and E, PDMs + US induced the highest apoptosis rate, free DTX and DMs produced similar apoptosis rates, and US irradiation monotherapy had no influence on apoptosis.

For cell cycle analysis, the PI/RNase method was employed and the remaining steps were the similar. In agreement with the cytotoxicity, cellular uptake, and apoptosis studies, the cell cycle analysis showed that cell cycle inhibition increased in response to different formulations (Fig. 3C and F). Hence, using the aforementioned data, it can be concluded that the PDMs combined with US irradiation increased drug uptake, inhibited the cell cycle, promoted apoptosis, and enhanced drug toxicity to the cells.

Tumour resistance to Paclitaxel family agent has been a problem troubling clinicians for a long time. Until studies on transcription and post-transcriptional mechanisms revealed that Paclitaxel family agent induces the expression of PD-L1 immunosuppressive molecules through the mitogen-activated protein kinase (MAPK) pathway²³. The evidence suggests patients may benefits from a synergy of docetaxel



and PD-1/PD-L1 checkpoint inhibitor, while PD-L1 is expressed in various tumor cells

24.

Enriched bio-distribution in melanoma tumour tissue mediated by PD-L1 and US targeting in vivo

Therapeutic efficacy and adverse effects could be influenced by the distribution and accumulation of various formulations in tumours and vital organs. DiR, a lipophilic fluorescent probe, was used to mark microbubbles directly. Free DiR, DiR-DMs, or DiR-PDMs were injected via the tail vein. DiR-PDMs combined with 10-minute-US irradiation was also investigated. The *in vivo* bio-distributions of different formulations were monitored by an IVIS Spectrum system. Compared with free DiR and DiR-DMs, DiR-PDMs exhibited an enhanced signal in tumour tissues *in vivo* and *ex vivo*, and this signal intensity was further enhanced with US irradiation (Fig. 5A). The signal of DiR-PDMs combined with US irradiation was found the strongest at the first hour. Among the groups, the DiR-PDMs group maintained the highest signal level. The DiR-PDMs showed a good targeting effect, and the signal reached a peak at 12 h. The DiR-DMs were enriched in tumours more than free DiR, which consistently exhibited a low signal intensity (Fig. 5B).

To further observe the distribution of formulations in organs after administration, tumour-bearing mice were sacrificed after the last imaging time point, and the tumours and all the vital organs (the heart, lungs, spleen, kidneys, and liver) were harvested for the following experiments. The *ex vivo* experimental results showed increased accumulation of DiR in tumour tissue (Fig. 5A). In addition, quantitative region of



interest analysis (Fig. 5C) showed that PDMs combined with US irradiation displayed the highest fluorescence efficiency, which might portend enhanced therapeutic effects. As predicted, US irradiation promoted rapid drug release in tumours, and the active targeting by the anti-PD-L1 mAb on the surface of PDMs promoted drug accumulation. Comparing the distributions of different drugs in major metabolic organs showed that the distribution of free drug in the liver was distinctly lower than that of the microbubbles. It is deduced that increasing the time between injections might reduce liver injury, and this was confirmed in the biotoxicity experiment.

Due to the side effects of immunochemotherapy, a variety of materials have been used as adjuncts²⁵⁻²⁸. The targeted drug delivery system of ultrasonic microbubbles, coupled with an antibody that targets a corresponding antigen overexpressed on tumour cells, provides a promising strategy for reducing the severe adverse effects associated with chemotherapeutic drugs^{29, 30}. The fabricated PDMs could effectively target the tumour tissue and thus reduce off-target toxicity. PD-L1 is highly expressed on the surface of various tumour cells and helps tumour cells evade antitumour immunity. Previous studies have indicated that anti-PD-L1 mAb-coupled drug delivery systems can target tumour cells³¹ and activate the immune system³², and this approach can synergize with chemotherapy. Therefore, it can be concluded that PDMs combined with US irradiation exhibited an increased drug concentration and extended drug duration in tumours and were therefore beneficial for therapeutic effects of increased strength and duration.

Inhibited tumour growth in a subcutaneous tumour model after treatments with



different microbubble formulations

A subcutaneous tumour model was established to evaluate the antitumour effects of various formulations of microbubbles *in vivo*. When the tumour volume reached 200 mm³, normal saline, free DTX, DMs, a free-drug combination, or PDMs were injected via the tail vein; PDMs combined with US irradiation were also investigated. Every 3 days, the mice were weighed, the tumour volumes were measured, and blood was obtained to assess liver and kidney functions. After all the treatments, the mice were sacrificed for subsequent histopathological study of the tumours and vital organs to evaluate efficacy and safety.

As shown in Fig. 6B-D, the PDMs combined with US irradiation group had the highest survival rate through the termination of experiment, and this group showed the best inhibition of tumour growth. The PDMs alone had a better therapeutic effect than the free-drug combination and ranked second. In addition, the synergistic therapy had more obvious efficacy than chemotherapy. The DMs produced slightly improved therapeutic effects on the tumour volume inhibition and survival rate. The difference in body weight was not obvious differences among the groups.

Apoptosis and proliferation in tumours were analysed via the TUNEL assay and CD31 and Ki67 immunohistochemistry (Fig.7 A-F). The data showed that the PDMs combined with US irradiation group had the highest apoptosis rate and lowest proliferation level. The trend in the data was in accordance with the tumour growth observations. The results for cleaved caspase-3, cleaved caspase-8, and cleaved caspase-9 in Western blot assays also revealed that the PDMs combined with US



irradiation group had the highest apoptosis rate (Fig. 8A-D).

It has been verified that US irradiation can enhance checkpoint inhibitor therapy³³. US irradiation combined with immunotherapeutic nanomaterials has been studied in colorectal cancer³³, B-cell lymphoma³⁴, and breast cancer³⁵. US irradiation combined with microbubble therapy for local lesions owns many advantages. The cavitation effect caused by microbubble rupturing under US irradiation can achieve high drug enrichment^{18, 36}. The sonoporation effect promotes drug uptake and enhances the delivery of small and large molecules^{37, 38}. Moreover, studies of US irradiation-enhanced microbubble tumour treatments indicated that this approach could induce rapid vascular damage and shut down blood flow³⁶. Our results demonstrated that PDMs combined with US irradiation can produce a strong antitumour effect.

Immune activation and cytokine production alleviation by microbubbles

To study the infiltration of immune cells into the tumour site after treatment, tumour-infiltrating lymphocytes (TILs) were harvested from tumours and analysed by immunofluorescence and flow cytometry on day 15 of the experimental process. The flow cytometry results also showed that CD8⁺ and CD4⁺ cell infiltration was approximately 4-fold greater in the PDMs combined with US irradiation group than in the control group (Fig. 8E and F). Immunofluorescence staining revealed that the tumours from the PDMs combined with US irradiation group were remarkably infiltrated by both CD8⁺ and CD4⁺ T cells, while untreated tumours exhibited limited infiltration (Fig. 8G).

We also observed that the level of TNF- α , which induces tumour cell apoptosis,



was increased in culture supernatants of tumour tissues after synergistic treatment (Fig. 8H). The immunosuppressive functions of TGF- β are correlated with malignancy in many cancers, the level of TGF- β was downregulated in response to the synergistic treatment (Fig. 8I). The expression of TNF- α and TGF- β after treatment with different formulations indicated that the synergistic treatment resulted in the best tumour suppression. In addition, the reduced levels of VEGF were observed (Fig. 8J), which play critical roles in angiogenesis, tumour growth and metastasis cancer. VEGF is also an important index for evaluating the growth of solid tumours. The PDMs combined with US irradiation produced the lowest VEGF expression; this result at the molecular level suggested that synergistic treatments could limit tumour growth.

Further antitumour efficacy in an orthotopic tumour model

We established orthotopic tumour models by injecting LLC cells in Matrigel under X-ray guidance (Fig. 9A and Fig S6). When the tumour volume reached 60 mm³, all the interventions were investigated. Increases in tumour volumes were obviously inhibited by PDMs combined with US irradiation therapy at the last follow-up CT scan (Fig. 9B and C), while the tumours in the other groups occupied almost the entire right lung. The synergistic therapy group also had a better health status and longer survival time than the other groups (Fig. 9D and E). Body weight declined gradually in all the groups except for the PDMs combined with US irradiation group, and this phenomenon was different from that observed in the subcutaneous tumour model. The possible reason is that although LLC cells have low invasiveness, pleural cavity occupation can affect cardiopulmonary function and blood oxygen levels, thereby affecting the health status



of the mice.

Since the lungs are air-filled cavities, lung diseases are often traditionally considered difficult to be treated with US irradiation. However, clinical studies have shown that US irradiation has obvious therapeutic efficacy in the treatment of lung diseases^{18,19} due to its ability to noninvasively mediate precise drug delivery. Here, the results of the orthotopic tumour experiment indicated that PDMs combined with US irradiation had good antitumour performance not only in subcutaneous tumour treatment but also in thoracic tumour treatment in mice.

Hence, US irradiation combined with microbubbles would be a promising noninvasive treatment, especially for lesions invading the chest wall. Patients with peripheral lung cancer are the ones most likely to benefit from this synergistic treatment. With the help of endoscopic and endobronchial US irradiation, this treatment may have a therapeutic effect on mediastinal lesions. The therapeutic efficacy of deep lung tumour therapy should be further explored. To our knowledge, this study is the first report in treating lung tumours with nanotechnology-mediated immunochemotherapeutic microbubbles combined with US irradiation.

Experimental

Materials

An anti-PD-L1 mAb was purchased from BioXCell, Inc. (Lebanon, NH, USA). DTX was purchased from J & K Scientific Co., Ltd. (Beijing, China). 1,2-Dipalmitoyl-sn-glycero-3-phosphocholine (DPPC), 1,2-dipalmitoyl-sn-glycero-3-phosphate (DPPA),



1,2-distearoyl-sn-glycero-3-phosphoethanolamine (DSPE), and 1,2-distearoyl-sn-glycero-3-phosphoethanolamine-N-[carboxy(polyethylene glycol)-2000] (DSPE-PEG-COOH) were purchased from A.V.T. Pharmaceutical Co., Ltd. (Shanghai, China). DSPE-PEG-FITC (molecular weight (MW): 2000) was purchased from Xi'an Ruixi Biological Technology Co., Ltd. Coumarin-6 (C6) was purchased from Yuanye Biotech, Inc. (Shanghai, China). 1,1'-Dioctadecyl-3,3',3',3'-tetramethylindotricarbocyanine iodide (DiR) was purchased from Aladdin Reagent Co., Ltd. (Shanghai, China). N-Hydroxysuccinimide (NHS) and N-(3-dimethylaminopropyl)-N'-ethylcarbodiimide hydrochloride (EDC) were purchased from Adamas-beta Inc. (Shanghai, China).

A cell counting kit-8 (CCK-8) assay and Annexin V-FITC/propidium iodide (PI) apoptosis detection, cell cycle detection, and VEGF, TNF- α , and TGF- β enzyme-linked immunosorbent assay (ELISA) kits were purchased from KeyGEN BioTECH Corp., Ltd. (Nanjing, China). Western blotting antibodies were purchased from Cell Signaling Technology (Beverly, MA, USA). Flow cytometry antibodies were purchased from eBioscience (eBioscience, Thermo Fisher Scientific, MA, USA).

Cell lines

LLC, A549, NCI-H460 [H460], and NCI-H1299 cells were kindly provided by Stem Cell Bank, Chinese Academy of Sciences. LLC cells were cultured in DMEM, A549 cells were cultured in F-12K medium, and NCI-H460 [H460] and NCI-H1299 cells were cultured in RPMI-1640 medium. All the media were supplemented with 10% foetal bovine serum (FBS), 100 U/mL penicillin, and 100 μ g/mL streptomycin. The cells were incubated at 37 °C with 5% CO₂.



Synthesis of microbubbles

Synthesis of basic microbubbles. DPPC: DPPA: DSPE: DTX in a weight ratio of 5.0 mg: 0.7 mg: 0.5 mg: 1.0 mg were dissolved in a solution of 6.0 mL of chloroform and 4.0 mL of methanol and then evenly ultrasonically mixed. The solvent was evaporated in the flask at 0.1 MPa and 42 °C to obtain a thin lipid film. When the residual chloroform evaporated at room temperature, the film was eluted with PBS. After the solution was concentrated to 1.5 mL, the dissolved gas in the solution was removed by ultrasonic clearing. Before starting the sonicator at 100 W and 4 °C for 10 min, we placed the probe approximately 3 mm below the liquid level and used SF₆ to completely remove the air. After separation by a dispersion and differential centrifugation method, relatively uniform DMs were obtained, and free DTX was washed away.

Synthesis of microbubbles loaded with an anti-PD-L1 mAb and DTX. Following the above-described method and replacing the 0.5 mg of DSPE with 1.8 mg of DSPE-PEG-COOH, microbubbles with a carboxyl group on the surface (DMs-COOH) were obtained. The DMs-COOH was dissolved in MES buffer (0.1 M, pH=5.5), and EDC and NHS were added and incubated for 30 minutes successively, so that the carboxyl terminal was activated. After washing the microbubbles three times with distilled water, the mass concentration of the DMs-COOH was determined by the freeze-drying method. We mixed the DMs-COOH and an equimolar amount of an anti-PD-L1 mAb in MES buffer (0.1 M, PH = 8.0) and incubated the mixture in a shaker at 4 °C overnight. We ultimately obtained PDMs after any unconjugated anti-PD-L1 mAb was washed away



by two rounds of centrifugation. C6-loaded microbubbles (C6-DMs and C6-PDMs) and DiR-loaded microbubbles (DiR-DMs and DiR-PDMs) were prepared with 1 mg of C6 or DiR added using the same method in the dark. All of the microbubbles were stored at 4 °C after sterilization by ⁶⁰Co irradiation (Jinpengyuan Irradiation Technology, Shanghai, China).

Characterization of the microbubbles

The particle sizes, size distributions, and zeta potentials of blank microbubbles (BMs), DMs, and PDMs were measured by a dynamic light scattering method on a ZetaPlus instrument (Brookhaven Instruments Corporation, NY, USA). The morphological characterization of the PDMs was performed with a scanning electron microscope (UltraPlus, Zeiss, Japan) after 200 μL of sample was drip-dried on silicon slices at room temperature for 48 h.

Drug loading efficiency and *in vitro* DTX release behaviours of microbubbles were detected by high-performance liquid chromatography (HPLC) with an Agilent 1200 HPLC system (Agilent, USA). We used acetonitrile/water (volume ratio of 1:1) as the mobile phase and Phenomenex C18 (4.6 mm × 250 mm, 5 μm) to separate samples. The samples were dissolved in the mobile phase under US, and then AUC was detected at 232 nm at 1 mL/min and 30 °C. According to our standard sample curve, we determined the concentration of DTX in each sample. The entrapment efficiency (EE%) and drug loading of DTX (DL%) were detected by HPLC and calculated using the following equations:

$$EE\% = W_{\text{encapsulated DTX}}/W_{\text{total feeding DTX}} \times 100\%;$$



$$DL\% = W_{\text{encapsulated DTX}}/W_{\text{total amount of microbubbles}} \times 100\%.$$

To investigate drug release behaviours, microbubbles and PBS were enclosed in dialysis bags (MWCO, 8000-14000 Da) with shaking in 2 L of PBS at 100 rpm and 37 °C with/without US irradiation (2.0 W/cm², 1 MHz, duty cycle 50% for 5 minutes). After 1 mL of dialysate water was removed from the container at predetermined intervals and stored at 4 °C for analysis, the same volume of PBS was used to replenish the sampled mixture. The release amount was measured by the same HPLC method described above. Three independent samples from each group were tested and analysed.

LSCM was hired to show the conjugation of a CY5-labelled anti-PD-L1 mAb with FITC-loaded microbubbles. The anti-PD-L1 mAb was labelled with CY5 according to the operation manual of the Lightning-Link Rapid Cyanine Dye 5 Kit (Expedeon, Heidelberg, Germany). DMs-FITC were prepared according to a method similar to the one described above.

To investigate the haemolytic effect of microbubbles, 50 µL of fresh anticoagulant-treated rabbit blood was mixed with (-) normal saline, BMs (w/v, 1 mg/mL), DMs (w/v, 1 mg/mL), PDMs (w/v, 1 mg/mL), or (+) pure water, and the samples were incubated at 37 °C for 60 minutes before centrifugation at 2000 rpm for 5 minutes. Then, the optical density (OD) of each supernatant solution was tested at 540 nm on a microplate reader (Thermo Scientific MultiskanFC, Thermo Fisher Scientific, MA, USA).

Toxicities of different microbubble formulations

All animal procedures were performed in accordance with the Guidelines for Care and



Use of Laboratory Animals of Southeast University and approved by the Animal Ethics Committee of Southeast University. C57BL/6 mice (6–8 weeks, $n = 20$) were randomly assigned to five groups for the toxicity test: the control group (normal saline), free DTX group, DM group, combination of free DTX and anti-PD-L1 mAb group, and PDM group. The drug was injected every three days for a total of five times as scheduled at a DTX dose of 2 $\mu\text{g/g}$. During the experimental schedule, the body weight of each animal was measured every three days, while blood biochemical indexes were evaluated weekly. The serum biochemical parameters including aspartate aminotransferase (AST), alanine aminotransferase (ALT), blood urea nitrogen (BUN), and creatinine levels were measured by a Hitachi 7020 automatic biochemical analyser.

Evaluation of contrast-enhanced US imaging

Solutions of BMs, DMs, and PDMs were ascertained by the freeze-drying method. Next, 1.0 mL of microbubbles (w/v, 1.0 mg/mL) or normal saline (as a control) was added to the holes in an agarose mould. One hundred microliters of BMs, DMs, or PDMs (w/v, 1 mg/mL) was intravenously injected into subcutaneous tumour model mice ($n = 3$) to evaluate the *in vivo* contrast imaging capability. Contrast-enhanced US images were obtained with an ultrasonic machine (Voluson E8, GE, USA) and analysed with QontraXt V3.06 (AMID-qX3, Bracco, Italy).

Influence of microbubbles on cell viability in vitro

The PD-L1 antigen expression of LLC, NCI-H460, NCI-H1299, and A549 cells were tested with an anti-CD274 (PD-L1, B7-H1) mAb (MIH5) labelled with PE (eBioscience, Thermo Fisher Scientific) on a flow cytometer (NovoCyte3000, ACEABiosciences,



Inc., CA, USA). All the analyses were processed with NovoExpress1.3.0 software.

View Article Online
DOI: 10.1039/C9BM01575B

The cytotoxicities of different microbubbles were measured using the CCK-8 method according to the manufacturer's protocol (KeyGEN BioTECH). LLC, NCI-H460, NCI-H1299, and A549 cells were seeded in 96-well plates with the corresponding incubation medium at a density of 5000 cells per well and incubated overnight. Then, 100 μ L of free DTX, BMs, DMs, PDMs, PDMs + US (US irradiation: 0.2 W/cm², 1 MHz, duty cycle 50% for 30 seconds after PDMs addition), or complete medium (control group) was added into each well so that the final concentration of DTX was 2 μ g/mL. After the cells were incubated for 24 h at 37 °C in a 5% CO₂ atmosphere, the supernatant was removed, and the cells were rinsed carefully with PBS twice, followed by the addition of RPMI 1640 medium (100 μ L) and CCK-8 (10 μ L) for 1 h. The OD was detected at 450 nm using a microplate reader. Relative cell viability (RCV) (%) was calculated as $RCV (\%) = OD_{test}/OD_{control} \times 100\%$.

Evaluation of specific DTX cellular uptake mediated by PD-L1

C6 was added to microbubbles to analyse cellular drug uptake. LLC cells were seeded in six-well plates with the corresponding incubation medium at a density of 5×10^5 cells per well. After incubating overnight, the cells were washed twice with PBS and treated with free C6, C6-DMs, C6-PDMs, or C6-PDMs + US at 37 °C for 2 h. US irradiation was implemented as described above. The cells were washed with PBS three times and fixed with 4% cold paraformaldehyde for 15 min. The cells were washed with PBS three times, and then a goat anti-rabbit IgG (H+L) secondary antibody conjugated with CY5 (Thermo Fisher Scientific) was added and incubated at room



temperature for 1 h. After the secondary antibody was removed with two washes, DAPI was added to the wells and incubated for 10 min. The cells were visualized with a fluorescence microscope (IX71, Olympus Corp., Tokyo, Japan). Then, we detached the cells with a trypsin solution and quantified the uptake efficiency on a flow cytometer.

Apoptosis assay and cell cycle analysis *in vitro*

Apoptosis induction was detected on a flow cytometer according to the manufacturer's protocol for Annexin V-FITC/PI Reagent (KeyGEN BioTECH). LLC cells were seeded in six-well plates at a density of 1×10^5 per well. After incubating overnight, the cells were treated with complete medium (control), US, DTX, DMs, PDMs, or PDMs + US. Twenty-four hours later, the cells were detached by 100 μ L of EDTA-free trypsin, stained and washed twice with PBS. Five hundred microliters of binding buffer was used to suspend the cells, 5 μ L of Annexin V-FITC and 5 μ L of PI were added and mixed, and the mixture was incubated for 15 min before analysis by flow cytometry.

For cell cycle analysis, the PI/RNase Cell Cycle Kit (KeyGEN BioTECH) was used according to the manufacturer's protocol. LLC cells were seeded in six-well plates at a density of 1×10^5 per well and incubated overnight. Then, the cells were starved in complete medium (2% FBS) for 24 h before treatment with complete medium (control), US, DTX, DMs, PDMs, or PDMs + US. Twenty-four hours later, the cells were collected, fixed in 75% ethanol at 4 °C overnight, washed twice with cold PBS, and stained with PI/RNase working buffer at room temperature for 30 min. Then, the cells were detected by flow cytometry.

Subcutaneous and orthotopic tumour models established with LLC cells



C57BL/6 mice (6–8 weeks) without black spots on the skin were used to establish subcutaneous tumour models. Each mouse was subcutaneously injected 100 μ L of LLC cells (1×10^7 /mL in PBS) in the right flank. The size of the orthotopic tumour was measured every other day and calculated with the following formula: Volume = (Length \times Width²)/2. Approximately 7 days later, when the tumour volume reached the predetermined size of 200 mm³, all the model mice were randomly assigned into groups.

Orthotopic tumour models were established by injection of 20 μ L of cell suspension into the right lung under imaging with an X-ray machine (WeMed Medical Equipment Co., Ltd., Beijing, China). The cell concentration was 1×10^7 /mL, and the cells were mixed with basement membrane matrices (Matrigel, BD Biosciences, NJ, USA). The injection device was constructed with a needle from a U-40 insulin injector (B. Braun, Melsungen AG, Germany) and an injector body from a 50- μ L microsyringe (Gaoge Industrial and Trading Co., Ltd., Shanghai, China). Orthotopic tumour size was monitored with a Hiscan XM Micro CT platform (Suzhou Hiscan Information Technology Co., Ltd., Suzhou, China). Approximately 5 days later, when the tumour volume reached the predetermined size of 60 mm³, all the model mice were randomly allocated into groups.

Assay of bio-distributions in mice treated with different microbubbles

Tumour-bearing mice were intravenously injected with free DiR, DiR-DMs, DiR-PDMs, or DiR-PDMs + US (n = 4 each group). Then, real-time images were acquired at different time points (1 h, 3 h, 6 h, 12 h, 24 h) via an IVIS Spectrum system (Caliper LifeSciences, PerkinElmer Inc, MA, USA) after the mice were anaesthetized with



isoflurane. Tumour tissue as well as the heart, lungs, liver, spleen, and kidneys were harvested for *ex vivo* imaging after the last imaging time point. The parameters for US irradiation were 2.0 W/cm², 1 MHz, and a duty cycle 50% for five minutes, which were repeatedly used in the following *in vivo* experiments. The images were analysed with Living Image 4.1 software (Caliper LifeSciences, PerkinElmer Inc., MA, USA).

In vivo antitumour study

To evaluate the antitumour efficacies of microbubbles, subcutaneous model mice were randomly divided into six groups (n = 6 each group) and intravenously injected 100 μ L of PBS, free DTX, free combination (DTX + anti-PD-L1 mAb), DMs, PDMs, or PDMs + US at a DTX dose of 2 μ g/g. Treatments were performed every 3 days. Body weight and tumour volume were measured every 3 days to observe antitumour efficacy and toxicity. All of the tumours, vital organs (the heart, liver, spleen, lungs, and kidneys), and blood were harvested. Tumour tissues were divided into three parts and processed for analyses: a real-time tissue homogenate for flow cytometry, a mass frozen at -80 $^{\circ}$ C for ELISA and Western blot analyses, and a 4% (w/v) paraformaldehyde-fixed mass for sectioning were prepared.

Tumour-infiltrating lymphocyte (TIL) suspensions were obtained by the mechanical dissociation and filtration method and stained with fluorochrome-conjugated mAbs specific for the cell surface markers CD4 (PE-CY5) and CD8a (PE), and an anti-rat IgG2a kappa antibody was used as an isotype control. The cells were analysed using a NovoCyte3000 flow cytometer with NovoExpress 1.3.0 software. In addition, immunofluorescence staining was used for double validation.



The antitumour efficacies of the microbubbles in the orthotopic tumour models were evaluated by CT scan, body weight, and survival rate statistics.

View Article Online
DOI: 10.1039/C9BM01575B

Statistical analysis

All statistical analyses were performed using SPSS 21.0 software and GraphPad Prism 8 software. Data are expressed as mean \pm standard deviation unless otherwise noted. An unpaired two-tailed *t*-test was used to compare between two groups. When comparing multiple groups, one-way ANOVA with the Newman-Keuls post hoc test was performed. Kaplan-Meier survival curves were analysed using the log-rank test with the Tukey post hoc test. Differences were considered statistically significant when $P < 0.05$. Statistical significance was noted as follows: # $P < 0.05$ and ## $P < 0.01$ compared with the control group, and * $P < 0.05$ and ** $P < 0.01$ between groups.

Conclusion

Here, we developed anti-PD-L1 mAb-conjugated and DTX-loaded multifunctional lipid-shelled microbubbles and verified that the anti-PD-L1 mAb and US irradiation could promote DTX uptake. We validated that a checkpoint inhibitor could be integrated into a therapeutic microbubble to produce a combination with synergistic effects. We also proved that US irradiation-mediated immunochemotherapeutic microbubble therapy could be used to treat lung cancer. This immunochemotherapeutic microbubble approach illustrates a successful treatment strategy that can be extended to other combinations based on clinically approved antibodies (e.g. anti-CTLA-4, anti-41-BB, or anti-TIM-3 antibodies) or traditional chemotherapeutic drugs (e.g.



doxorubicin, pemetrexed, or gemcitabine). The synergistic therapy of US combined with immunochemotherapeutic microbubbles might be a promising treatment for a variety of malignancies, potentially leading to the development of a new approach for combination immunotherapy.

Associated content

Supporting Information

Supplemental results and methods are depicted in the Supporting Information Table S1 Characteristics of different microbubbles. Table S2 Encapsulation efficiency and drug-loading efficiency of microbubbles. Fig. S1. Haemolysis tests of BMs, DMs, and PDMs. Fig. S2. Mouse body weight (A) as well as AST (B), ALT (C), creatinine (D) and blood urea nitrogen (E) levels were monitored over the course of treatment. Fig. S3. HE assessment of the heart, liver, lungs, spleen, and kidneys. Fig. S4. Flow cytometry assay of C6 uptake by LLC cells treated with different formulations. Supplementary Fig. S5. Flow cytometry analysis of CD4+ and CD8+ TIL numbers after treatments. Fig. S6. LLC cells with Matrigel were injected into the right lung of C57BL/6 mice under X-ray guidance to establish an orthotopic tumour model.

Author information

Corresponding Author

* Dr. Jinhe Guo, Email: jinheguo@sina.com

Author Contributions



† These authors contributed equally to this work.

View Article Online
DOI: 10.1039/C9BM01575B

Conflicts of interest

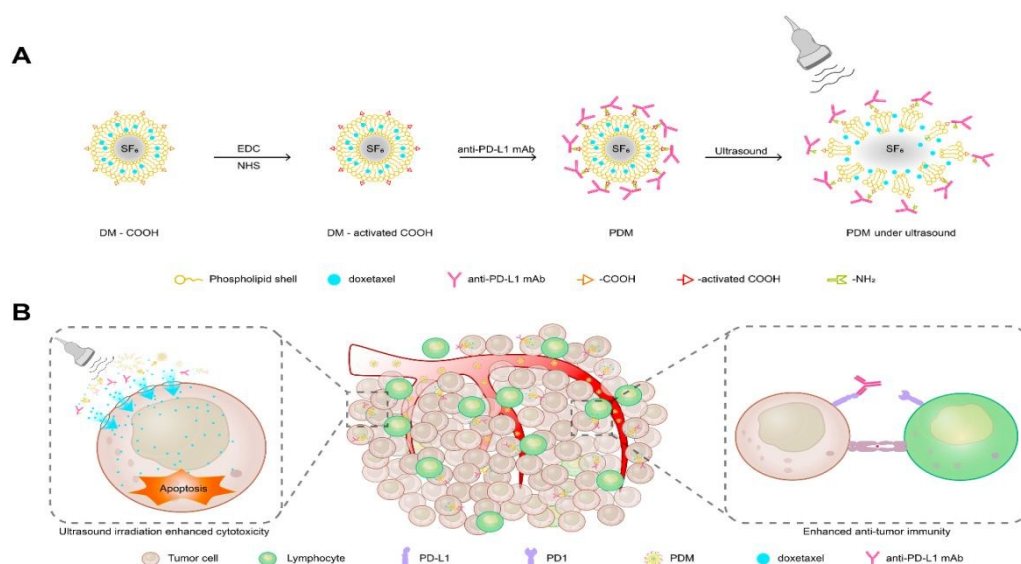
The authors have declared that no competing interest exists.

Acknowledgements

This research was financially supported by the National Natural Science Foundation of China (No. 81671795, No. 81971628, and No. 81971716). We are grateful to Jiangsu Key Laboratory of Molecular and Functional Imaging for assistance with material synthesis, material characterization, and biological integrated experiments.

Figures

Fig. 1. Novel microbubbles combining DTX antitumour activity with PD-L1 blockade in the context of ultrasound irradiation. (A) Schematic diagram showing the preparation of DTX and anti-PD-L1 mAb-co-loaded microbubbles. (B) Scheme of synergistic chemotherapy and immunotherapy under ultrasound irradiation for tumour treatment.



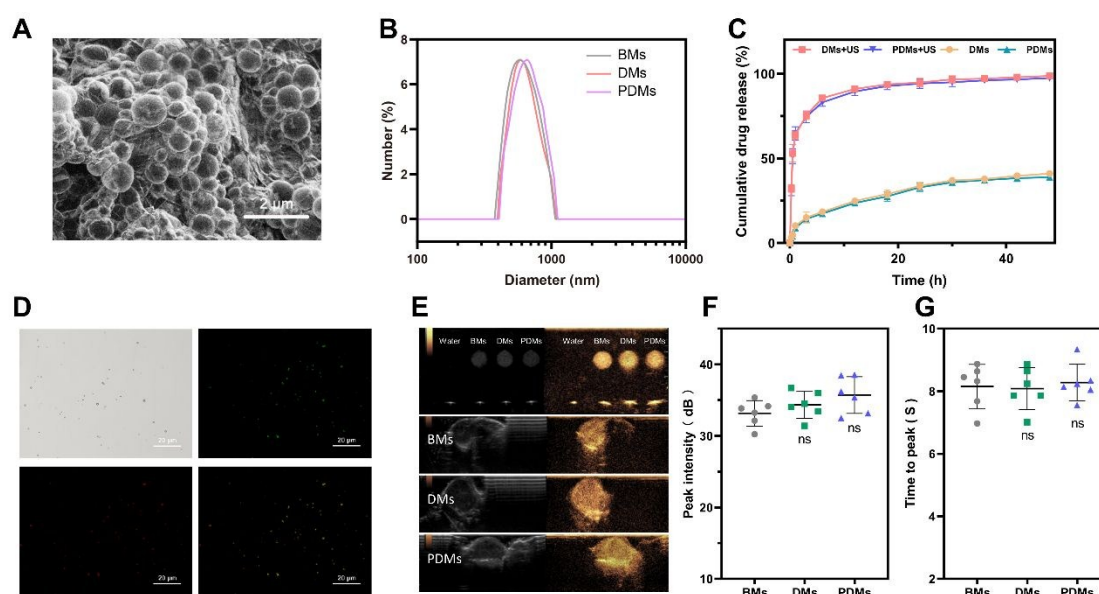


Fig. 2. Characterization of docetaxel and anti-PD-L1 mAb-co-loaded microbubbles. (A) SEM image of PDMs, scale bar = 2 μm. (B) Particle size distributions. (C) *In vitro* cumulative drug release by different bubbles with or without US irradiation. (D) CLSM images of docetaxel and CY5-labelled anti-PD-L1 mAb-co-loaded microbubbles with a shell containing FITC, scale bar = 20 μm. (E) *In vitro* and *in vivo* contrast effects of microbubbles. (F) Peak intensity of *in vivo* imaging of microbubbles. (G) Time to peak *in vivo* imaging of microbubbles. The data in 2F and 2G are expressed as the mean ± s.d.; n = 6 independent samples, analysed using one-way ANOVA with the Newman-Keuls post hoc test. ns indicates $P > 0.05$ compared with the BMs group.

BMs (blank microbubbles), DMs (docetaxel-loaded microbubbles), PDMs (docetaxel and anti-PD-L1 mAb-co-loaded microbubbles), US (ultrasound irradiation).



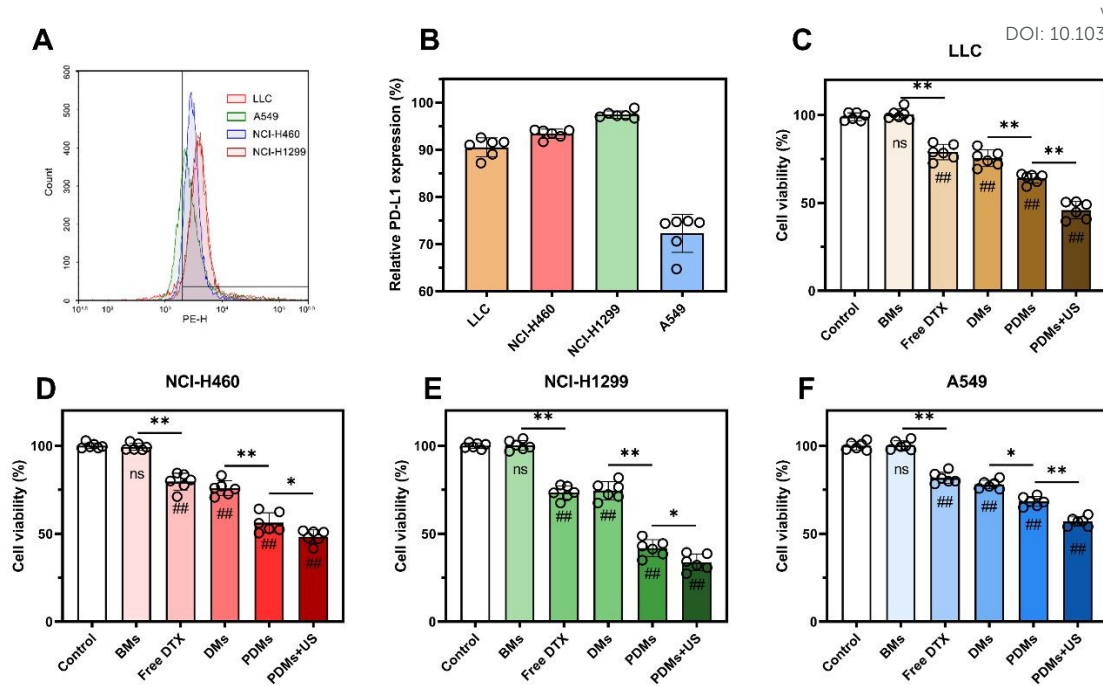


Fig. 3. PD-L1 expression of LLC, A549, NCI-H460, and NCI-H1299 cells and the toxicity of microbubbles to tumour cells. (A) Flow cytometry was used to assess the PD-L1 expression profiles of cells. (B) LLC, NCI-H460, and NCI-1299 cells showed relatively high PD-L1 expression, while A549 cells showed the lowest PD-L1 expression. (C-F) A CCK-8 assay was used to determine the cell viabilities of tumour cells incubated with different formulations for 24 h. The results in B-F are expressed as the mean \pm s.d.; $n = 6$ independent samples, analysed using one-way ANOVA with the Newman-Keuls post hoc test. $\#P < 0.05$ and $\#\#\#P < 0.01$ compared with the control group (without microbubbles); $*P < 0.05$ and $**P < 0.01$ for comparisons among groups.



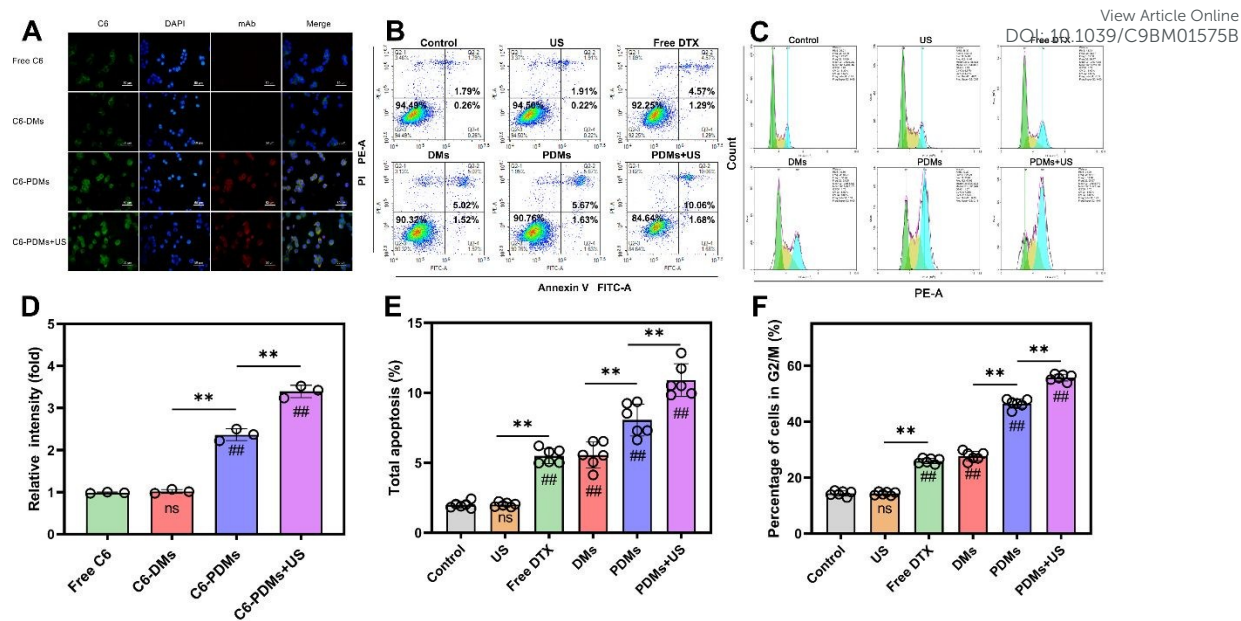


Fig. 4. Cellular uptake, apoptosis, and cell cycle inhibition of LLC cells given different treatments. (A, D) Fluorescence images taken after a four-hour incubation with free C6, C6-DMs, C6-PDMs, or C6-PDMs with 30 seconds of ultrasound irradiation; DAPI, blue; C6, green; and a goat anti-rat secondary antibody, red; scale bar = 50 μm ; $n = 3$. The data were processed using ImageJ software. (B, E) Cell apoptosis study of LLC cells after incubation. The cells were treated with ultrasound irradiation, free DTX, DMs, PDMs, or PDMs + US, and the total apoptosis rate was analysed. (C, F) Cell cycle inhibition study of LLC cells treated with ultrasound irradiation, free DTX, DMs, PDMs, or PDMs with ultrasound irradiation after an incubation. Data are shown as the mean \pm s.d.; $n=6$ independent samples, analysed using one-way ANOVA with the Newman-Keuls post hoc test. # $P < 0.05$ and ## $P < 0.01$ compared with the control group (without microbubbles), * $P < 0.05$ and ** $P < 0.01$ for comparisons among groups.

C6 (Courmarin-6), C6-DMs (Docetaxel and Courmanrin-6-co-loaded microbubbles), C6-PDMs (Courmanrin-6, docetaxel and anti-PD-L1 mAb-co-loaded microbubbles).



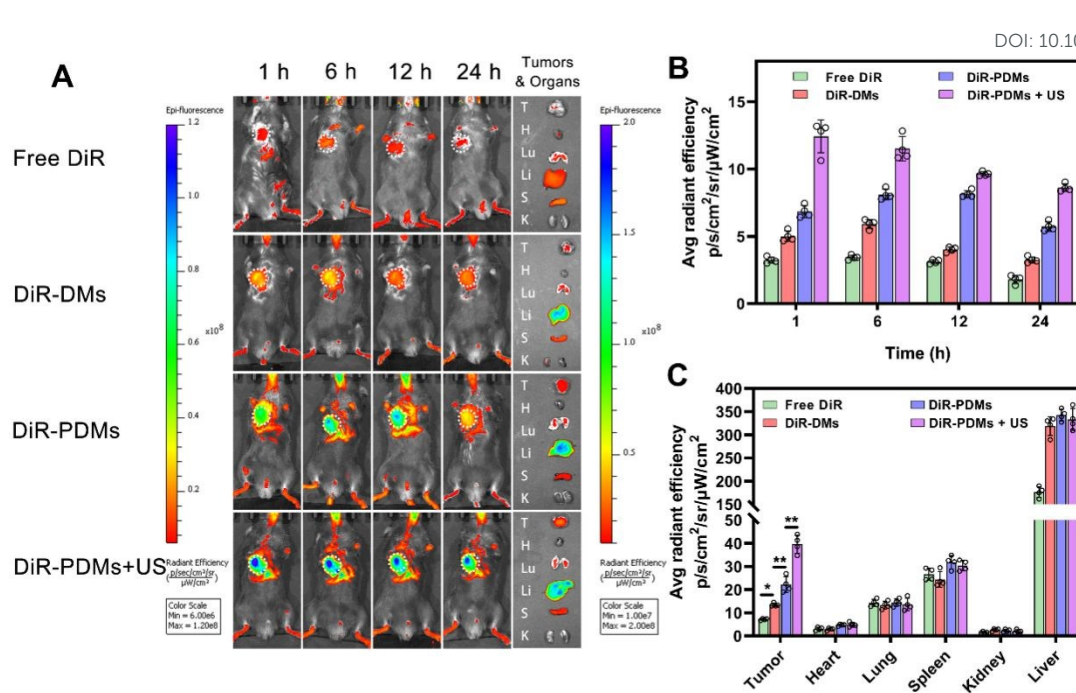


Fig. 5. IVIS images of mice treated with different formulations. (A) Fluorescence images of mice-bearing LLC melanoma at 1, 6, 12, and 24 h after free DiR, DiR-DMs, or DiR-PDMs treatment with/without ultrasound irradiation. Tumours and major organs were harvested after the last imaging session. (B) Statistical analysis of the superficial ROI average radiant efficiency. (C) Statistical analysis of the average radiant efficiency of the organs and tumours. Data are shown as the mean \pm s.d.; $n = 4$ biologically independent mice, analysed using one-way ANOVA with the Newman-Keuls post hoc test. $*P < 0.05$ and $**P < 0.01$ among groups.



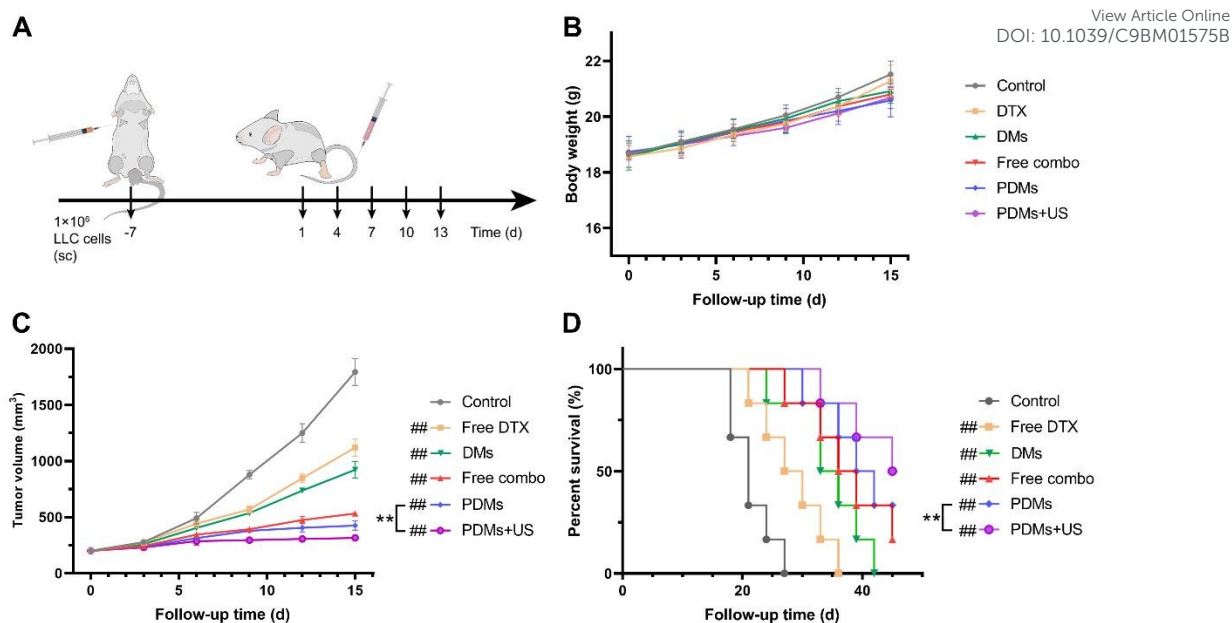


Fig. 6. Treatment with PDMs and ultrasound irradiation enhanced tumour inhibition in an LLC subcutaneous tumour model. (A) C57BL/6 mice were subcutaneously injected LLC cells on day -7. When tumour volume reached 200 mm^3 , the mice received different therapeutic formulations. (B) Body weight, (C) tumour volume, and (D) survival were analysed. The data in B and C are expressed as the mean \pm s.d.; $n = 6$ biologically independent animals. $\#P < 0.05$ and $\#\#P < 0.01$ compared with the control group (normal saline); $*P < 0.05$ and $**P < 0.01$ between groups compared using a paired two-way Student's t -test. The log-rank test followed by Tukey's post hoc test was performed to determine statistical significance in D; $n = 6$ biologically independent animals. $\#P < 0.05$ and $\#\#P < 0.01$ compared with the control group, $*P < 0.05$ and $**P < 0.01$ compared with the control group (normal saline).



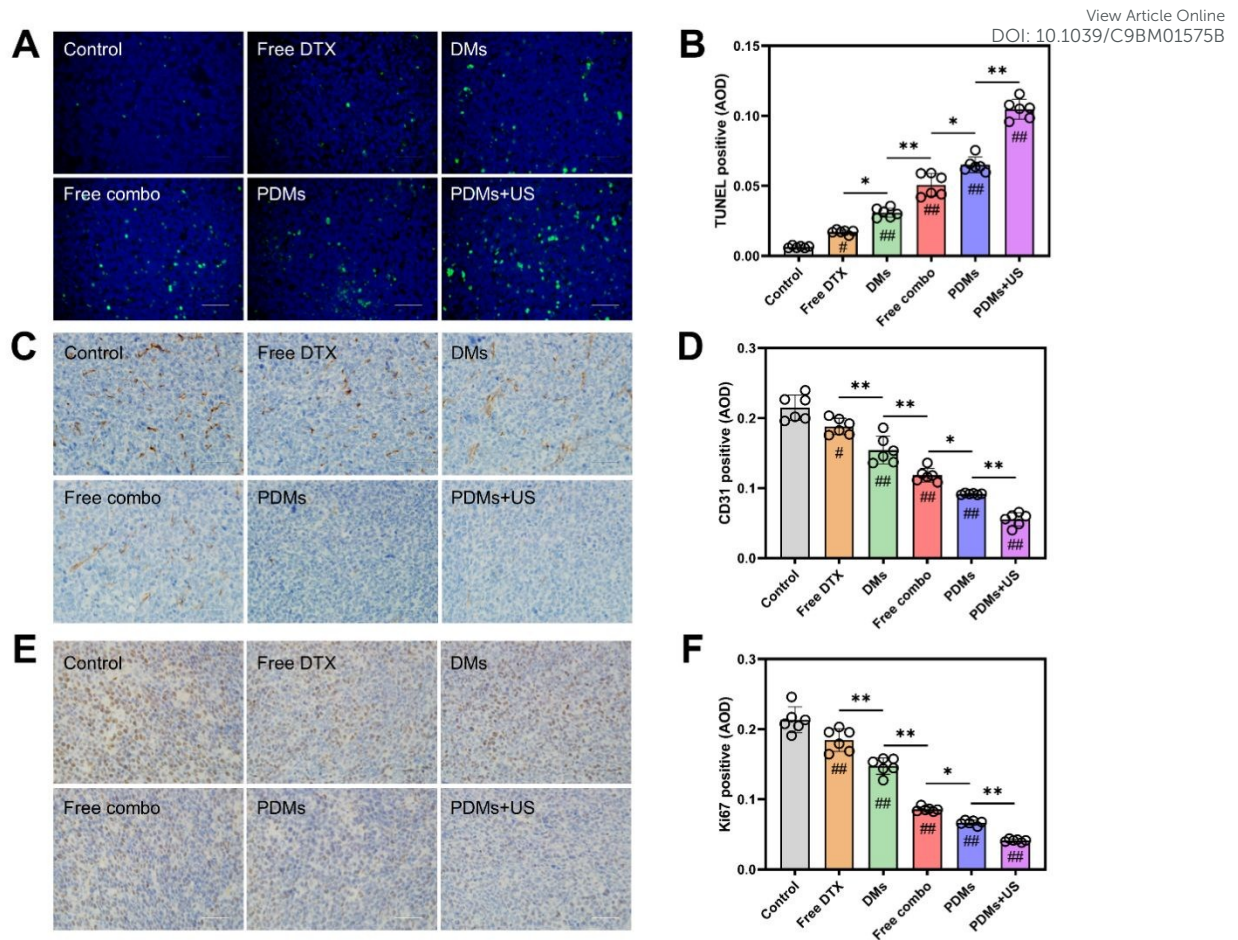


Fig. 7. TUNEL staining and immunohistochemical staining for CD31 and Ki67 in tumour sections. (A) TUNEL-stained merged image (apoptotic cells are shown in green) and statistical analysis of **(B)** the positive rate of TUNEL staining.

Immunohistochemical staining for **(C)** CD31 and **(E)** Ki67 in tumour sections; angiogenic cells and proliferating cells are shown in brown. Scale bar = 200 μm .

Statistical analysis of the positive rates for **(D)** CD31 and **(F)** Ki67 staining. Data were processed by ImageJ software and are expressed as mean \pm s.d.; $n = 6$, analysed using one-way ANOVA with the Newman-Keuls post hoc test. # $P < 0.05$ and ## $P < 0.01$ compared with the control group (without microbubbles); * $P < 0.05$ and ** $P < 0.01$ among groups.



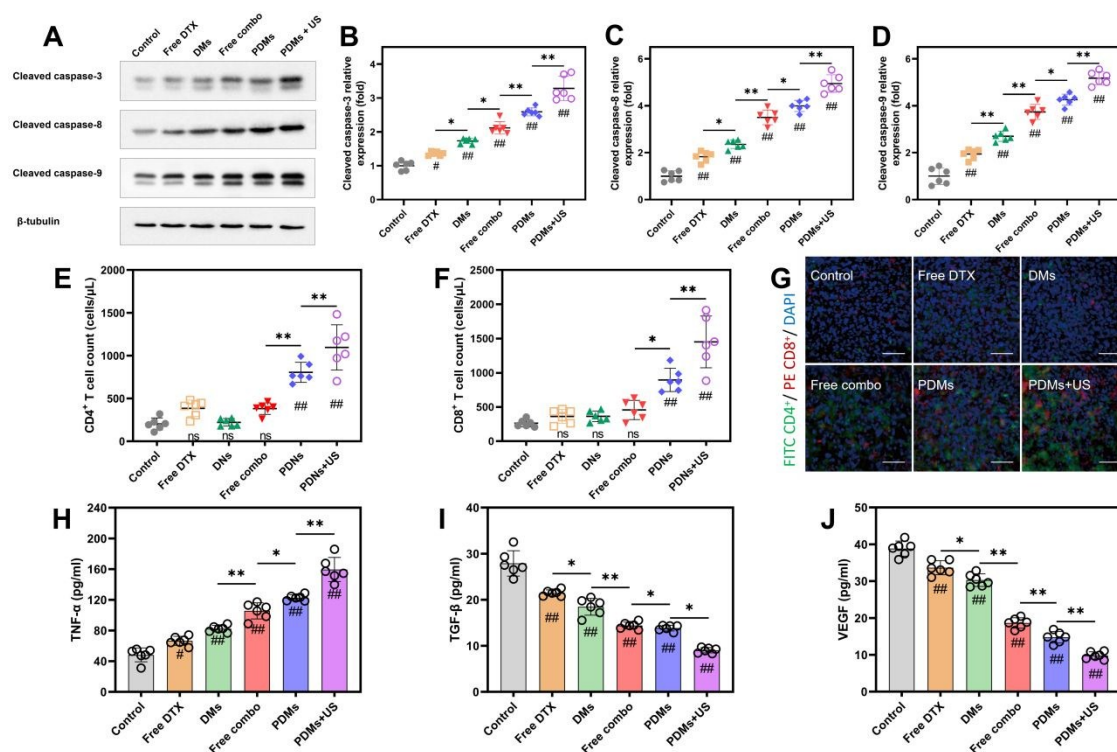


Fig. 8. Changes in Western blot assays, TIL levels and cytokine levels at 15 days after the first treatment. (A-D) Western blot data for apoptosis-related proteins showed the expression of proapoptotic proteins. Data were processed using ImageJ software. (E, F) Flow cytometry analysis determined the numbers of CD4⁺ and CD8⁺ TILs increased after treatments, counts of each subset were gated from CD45⁺ lymphocytes. (G) Fluorescence micrographs of tumour sections show CD4⁺ (red) and CD8⁺ (green) TILs and DAPI staining (blue); scale bar = 200 μm. The levels of cytokines, including TNF-α (H), TGF-β (I) and VEGF (J), in tissue culture supernatants were determined. PDMs + US significantly increased TIL numbers and improved pro-inflammatory cytokine levels. The results are expressed as mean ± s.d.; n = 6 biologically independent mice, analysed by one-way ANOVA with the Newman-Keuls post hoc test. #*P* < 0.05 and ##*P* < 0.01 compared with the control group (normal



saline); * $P < 0.05$ and ** $P < 0.01$ among groups.

View Article Online
DOI: 10.1039/C9BM01575B

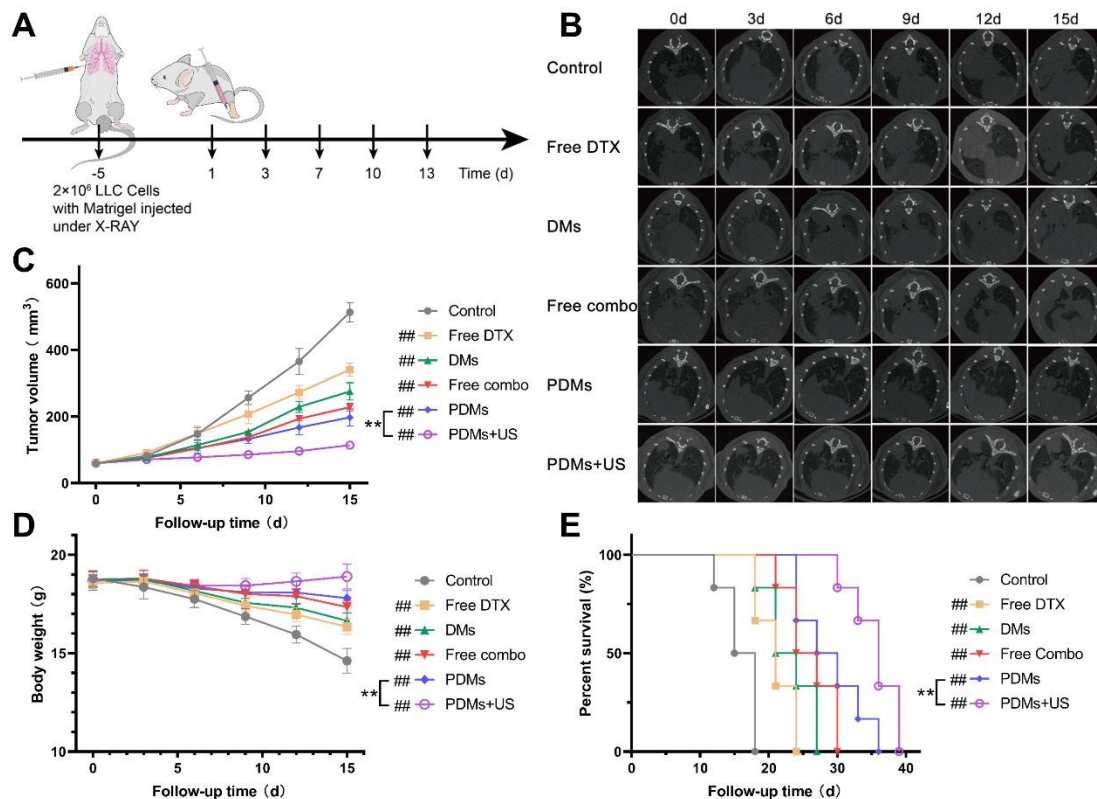


Fig. 9. Different therapeutic formulations were tested in an orthotopic LLC tumour model. (A) Twenty microliters (containing 2×10^6 LLC cells with Matrigel) were injected into the right lung of C57BL/6 mice under X-ray guidance on day 5. When tumour volume reached 60 mm^3 , the mice received different therapeutic formulations. Follow-up analyses (B) CT scanning results, (C) tumour volume, (D) body weight, and (E) survival. The data in C and D are expressed as mean \pm s.d.; $n = 6$ biologically independent mice. # $P < 0.05$ and ## $P < 0.01$ compared with the control group (normal saline); * $P < 0.05$ and ** $P < 0.01$ between groups using a paired two-way Student's t -test. The log-rank test was performed followed by Tukey's post hoc test to determine statistical significance in E; $n = 6$ biologically independent mice. # $P < 0.05$ and ## $P < 0.01$ compared with the control group (normal saline); * $P < 0.05$ and



**** $P < 0.01$ between groups.**

References:

1. R. L. Siegel, K. D. Miller and A. Jemal, *CA Cancer J Clin*, 2019, 69, 7-34.
2. R. Alanni, J. Hou, H. Azzawi and Y. Xiang, *IET Syst Biol*, 2019, 13, 129-135.
3. J. J. Havel, D. Chowell and T. A. Chan, *Nat Rev Cancer*, 2019, 19, 133-150.
4. S. L. Topalian, J. M. Taube, R. A. Anders and D. M. Pardoll, *Nat Rev Cancer*, 2016, 16, 275-287.
5. A. H. Sharpe and K. E. Pauken, *Nat Rev Immunol*, 2018, 18, 153-167.
6. R. S. Herbst, P. Baas, D. W. Kim, E. Felip, J. L. Perez-Gracia, J. Y. Han, J. Molina, J. H. Kim, C. D. Arvis, M. J. Ahn, M. Majem, M. J. Fidler, G. de Castro, Jr., M. Garrido, G. M. Lubiniecki, Y. Shentu, E. Im, M. Dolled-Filhart and E. B. Garon, *Lancet*, 2016, 387, 1540-1550.
7. NCCN, *Journal*, 2019.
8. M. Nagasaka and S. M. Gadgeel, *Expert Rev Anticancer Ther*, 2018, 18, 63-70.
9. C. Schmidt, *Nature*, 2017, 552, S67-s69.
10. J. J. Moslehi, J. E. Salem, J. A. Sosman, B. Lebrun-Vignes and D. B. Johnson, *Lancet*, 2018, 391, 933.
11. S. Baxi, A. Yang, R. L. Gennarelli, N. Khan, Z. Wang, L. Boyce and D. Korenstein, *Bmj*, 2018, 360, k793.
12. G. Quintero Aldana, M. Salgado, S. Candamio, J. C. Mendez, M. Jorge, M. Reboredo, L. Vazquez Tunas, C. Romero, M. Covela, A. Fernandez Montes, M. Carmona, Y. Vidal Insua and R. Lopez, *Clin Transl Oncol*, 2019, DOI: 10.1007/s12094-019-02151-6.
13. S. Kanda, K. Goto, H. Shiraishi, E. Kubo, A. Tanaka, H. Utsumi, K. Sunami, S. Kitazono, H. Mizugaki, H. Horinouchi, Y. Fujiwara, H. Nokihara, N. Yamamoto, H. Hozumi and T. Tamura, *Ann Oncol*, 2016, 27, 2242-2250.
14. N. Li, L. Han and H. Jing, *Exp Ther Med*, 2017, 14, 3768-3773.
15. S. R. Sirsi, C. Fung, S. Garg, M. Y. Tianning, P. A. Mountford and M. A. Borden, *Theranostics*, 2013, 3, 409-419.
16. R. Cavalli, M. Soster and M. Argenziano, *Ther Deliv*, 2016, 7, 117-138.
17. M. Gutierrez, M. Tardella, L. Rodriguez, J. Mendoza, D. Clavijo-Cornejo, A. Garcia and C. Bertolazzi, *Radiol Med*, 2019, DOI: 10.1007/s11547-019-01053-5.
18. M. G. Sugiyama, V. Mintsopoulos, H. Raheel, N. M. Goldenberg, J. E. Batt, L. Brochard, W. M. Kuebler, H. Leong-Poi, R. Karshafian and W. L. Lee, *Am J Respir Crit Care Med*, 2018, 198, 404-408.
19. B. Lu, L. Sun, X. Yan, Z. Ai and J. Xu, *Med Oncol*, 2015, 32, 345.
20. S. Xenariou, U. Griesenbach, H. D. Liang, J. Zhu, R. Farley, L. Somerton, C. Singh, P. K. Jeffery, S. Ferrari, R. K. Scheule, S. H. Cheng, D. M. Geddes, M. Blomley and E. W. Alton, *Gene Ther*, 2007, 14, 768-774.
21. C. M. Schoellhammer, G. Y. Lauwers, J. A. Goettel, M. A. Oberli, C. Cleveland, J. Y. Park, D. Minahan, Y. Chen, D. G. Anderson, A. Jaklenc, S. B. Snapper, R. Langer and G. Traverso, *Gastroenterology*, 2017, 152, 1151-1160.
22. W. Sun, Z. Li, X. Zhou, G. Yang and L. Yuan, *Drug Deliv*, 2019, 26, 45-50.



23. W. Gong, Q. Song, X. Lu, W. Gong, J. Zhao, P. Min and X. Yi, *Journal of chemotherapy* (Florence, Italy), 2011, 23, 295-299. View Article Online
DOI:10.1039/C9BM01575B
24. S. C. Liang, Y. E. Latchman, J. E. Buhlmann, M. F. Tomczak, B. H. Horwitz, G. J. Freeman and A. H. Sharpe, *European journal of immunology*, 2003, 33, 2706-2716.
25. C. S. Chiang, Y. J. Lin, R. Lee, Y. H. Lai, H. W. Cheng, C. H. Hsieh, W. C. Shyu and S. Y. Chen, *Nat Nanotechnol*, 2018, 13, 746-754.
26. W. J. Wan, C. X. Qu, Y. J. Zhou, L. Zhang, M. T. Chen, Y. Liu, B. G. You, F. Li, D. D. Wang and X. N. Zhang, *Int J Pharm*, 2019, 566, 731-744.
27. R. Kuai, W. Yuan, S. Son, J. Nam, Y. Xu, Y. Fan, A. Schwendeman and J. J. Moon, *Sci Adv*, 2018, 4, eaao1736.
28. Z. S. Dunn, J. Mac and P. Wang, *Biomaterials*, 2019, 217, 119265.
29. E. C. Abenojar, P. Nittayacharn, A. C. de Leon, R. Perera, Y. Wang, I. Bederman and A. A. Exner, *Langmuir*, 2019, 35, 10192-10202.
30. S. Zhou, S. Zheng, Y. Shan, L. Li, X. Zhang and C. Wang, *Oncol Rep*, 2016, 35, 801-808.
31. S. Xu, F. Cui, D. Huang, D. Zhang, A. Zhu, X. Sun, Y. Cao, S. Ding, Y. Wang, E. Gao and F. Zhang, *Int J Nanomedicine*, 2019, 14, 17-32.
32. Z. Gu, Q. Wang, Y. Shi, Y. Huang, J. Zhang, X. Zhang and G. Lin, *J Control Release*, 2018, 286, 369-380.
33. S. Bulner, A. Prodeus, J. Garipey, K. Hynynen and D. E. Goertz, *Ultrasound Med Biol*, 2019, 45, 500-512.
34. S. Zheng, D. Song, X. Jin, H. Zhang, M. Aldarouish, Y. Chen and C. Wang, *Nanomedicine (Lond)*, 2018, 13, 297-311.
35. W. Sun, Y. Du, X. Liang, C. Yu, J. Fang, W. Lu, X. Guo, J. Tian, Y. Jin and J. Zheng, *Biomaterials*, 2019, 217, 119264.
36. D. E. Goertz, M. Todorova, O. Mortazavi, V. Agache, B. Chen, R. Karshafian and K. Hynynen, *PLoS One*, 2012, 7, e52307.
37. H. Yu, Z. Lin, L. Xu, D. Liu and Y. Shen, *Ultrasonics*, 2015, 61, 136-144.
38. B. L. Helfield, X. Chen, B. Qin, S. C. Watkins and F. S. Villanueva, *Ultrasound Med Biol*, 2017, 43, 2678-2689.

